

Dead time duration and active reset influence on the afterpulse probability of InGaAs/InP single-photon avalanche diodes

A. V. Losev^{1,2,3,4}, V. V. Zavodilenko^{1,4}, A. A. Koziy^{1,4}, A. A. Filyaev^{1,4,5}, K. I. Khomyakova⁶,
Y. V. Kurochkin^{1,3,4}, A. A. Gorbatshevich^{2,7}

¹“QRate” LLC, St. Novaya, d. 100, Moscow region, Odintsovo, Skolkovo, 143026, Russia.

²National Research University of Electronic Technology MIET, Shokin Square, 1, Zelenograd, 124498, Russia.

³National University of Science and Technology MISIS, Leninsky prospect, 4, Moscow, 119333, Russia.

⁴NTI Center for Quantum Communications, National University of Science and Technology MISiS, Leninsky prospekt 4, Moscow, 119049, Russia.

⁵Bauman Moscow State Technical University, 2nd Baumanskaya st., 5, Moscow, 105005, Russia.

⁶National Research Tomsk State University, Lenin Av. 36, Tomsk, 634050, Russia.

⁷P.N. Lebedev Physical Institute of the Russian Academy of Sciences, Leninsky prospect, 53, Moscow, 119333, Russia.

Abstract—We have performed a detailed study of the dependence of afterpulse probability in InGaAs/InP sine-gated SPAD on the dead time and the existing approach for its implementation. We demonstrated an electrical scheme combining sinusoidal gating and active reset. We have shown when such solutions are beneficial from the key distribution point of view and enough to use a simple scheme with a snatching comparator. We have also proposed a precise method for measuring the afterpulse and presented a model describing the non-markovian dynamic of this effect. We have demonstrated that our afterpulsing measurement approach makes these measurements less dependent on the parameters of the flow of the diode and the laser pulses power changes, in contrast to the other methods considered in this paper.

Index Terms—Single-photon detector, single-photon avalanche diode, dead time, afterpulse probability.

I. INTRODUCTION

DETECTORS based on superconducting nanowires (SNSPD) [1] and single photon avalanche diodes (SPAD) [2] have proven themselves in the best way as single-photon detectors (SPDs). Each of the implementations has both its advantages and disadvantages. SNSPD has high probability of photon detection and low noise level, but it is large and quite expensive due to usage of helium cryostat [3]. SPAD-based SPDs have small size and low cost, but detection probability is relatively low, and noise characteristics are high. In quantum key distribution (QKD), both first and second types of SPD have found their application [4], [5]. It is advisable to use SNSPD for key distribution over long distances, both over fiber and open space. SNSPD based QKD was able to demonstrate key distribution distance records [6]. It is advisable to use SPAD-based SPD in small-sized industrial installations [7] that distribute the key within one city or even one building since the loss of photons in the line is minimal and the key generation rate is relatively high.

One of the big problems of the QKD is the difficulty of determining the secrecy of the generated key. In contrast to classical cryptographic algorithms, in which applied mathematical transformations strictly determine confidentiality of the key, quantum cryptography depends on the installation’s physical parameters [8]. Thus, calculated key secrecy can be selected pessimistically, which will significantly reduce key generation rate or optimistically, which will endanger security of subsequently encrypted data. For this reason, development of methods for accurate determination of the parameters of SPD is an actual task that can significantly increase the efficiency of the QKD installation as a whole [9].

In SNSPD with adequate control electronics, there are no effects associated with previous triggers [10]. Therefore, we can consider all processes as Markovian [11]. There is “memory” of earlier triggers in SPAD-based SPDs – the processes have more complicated influence on counting statistics [12], and the construction of a global SPD model becomes complicated. Charges captured by the traps cause this memory. These charges relax after a particular time and can lead to the formation of an avalanche and the subsequent detector’s triggering, and are called afterpulses [13].

For detectors of 1550 nm wavelength photons, based on InGaAs/InP SPAD, total relaxation time is about 1 – 50 μ s at a temperature of about $-100 - -50$ °C. For Si-based photon detectors for visible radiation, full relaxation time is about 200 ns [14]. To overcome afterpulsing, the following methods are used: usage of SPD circuits with dead time – the time during which the detector is not able to detect photons after the previous detection event; lowering avalanche growing time by fast quenching. We can use high dead time, but SPDs used in QKD receive significant restrictions on the limiting operating frequencies, which harms the installation’s efficiency as a whole. Therefore, to obtain the SPD’s highest efficiency for the QKD application, the dead time value is reduced to

1–10 μs while sacrificing QBER but gaining maximum count rate, which is especially important for short distances QKD [15].

Two articles inspire the theoretical part of our work: [16], and [17], where authors try to describe the recurrent nature of the afterpulsing effect and its non-markovian properties. Our article used more rigorous probability equations, making our model more general, for example, for very different count rates. We developed an accurate method for calculating the detector's afterpulse probability from counting statistics.

In this work we observe only the dead time approach for afterpulse control. We investigated two possible technical realizations of the dead time: it includes comparator latching (passive quenching and reset) as well as active bias lowering (passive-active quenching and reset). We analyzed these two methods and made recommendations on using one of them in different practical cases. We made recommendations for setting time parameters of latching the comparator based on statistical data analysis and the physics of the processes.

II. COMMON (STANDARD) AFTERPULSE MODELS

There are the most popular methods for determining of afterpulsing: Bethune method [18], [19], Yuan method [20]–[22], coincidence method [23]–[25], double-pulse method [26]–[28], autocorrelation method [16], [29], Klyshko method [30]–[33]. The double-pulse method can be used only for changeable gates, like square gates, and is not applicable for sine-gating, and we do not overview it here. The autocorrelation method can be effectively used only with a multichannel autocorrelator device, and we do not observe this method due to its absence. The Klyshko method was used as a true single-photon source based on a parametric downconversion effect instead of a simple laser with multiphoton states. However, we cannot observe this method because we do not have a true single-photon source. We will briefly describe the essence of each of the other common methods.

The Bethune, Yuan, and coincidence methods are pretty similar; however, they differ in histogram collections and postprocessing approaches. We need to collect two histograms in each method: with and without light illumination. In figure 1 we collect the histograms for each of the methods.

In the Bethune method, we need to set up the frequency of laser pulses as half of the gating pulses. For our SPD gating frequency $f_g = 312.5$ MHz, we set up laser pulse frequency to $f_l = 156.25$ MHz. For more details about our custom SPDs and measuring stand, see the section IV. We need to collect histograms of detector triggers dependent on time with a resolution, preferably more than ten bins per gate, to make different gates distinguishable on histograms (as in the Yuan method). Afterpulsing obtaining with postprocessing of such histograms (see figure 1 a):

$$P_{ap} = \frac{R_{ni} - R_{dark}}{R_{de}}, \quad (1)$$

where P_{ap} is the afterpulse probability, and with illumination: R_{ni} is count rate in non-illuminated gate R_{de} is count rate in two consecutive gates; without illumination: R_{dark} is count rate in gate.

In the Yuan method, we can set laser pulses frequency multiple of gate frequency, for example, one-fiftieth: $f_l = 6.25$ MHz. We collect the similar histogram as in the Bethune method (see figure 1 b), and post-process it:

$$P_{ap} = \frac{R_{ni} - R_{dark}}{R_{de}^c - R_{ni}} \cdot \frac{f_g}{f_l}, \quad (2)$$

where R_{ni} is the specific bin after the illuminated gate, R_{de}^c are the coincidence triggers of SPD and laser pulse arriving, i.e., count rate in the illuminated gate.

The main disadvantage of this method is that we are looking at afterpulsing only by one specific gate to calculate R_{ni} . However, afterpulsing has an exponential distribution over the gate number, and if we get another gate with own R_{ni} , then we obtain another result.

In the coincidence method, we can solve the issue of the Yuan method. For measuring, we get the same laser pulse repetition rate: $f_l = 6.25$ MHz, and collect the histogram over the sweep, equal to one laser pulse period. We can use less resolution in this method because gates distinguishability is unimportant. We can process histogram (see figure 1 c) as follows:

$$P_{ap} = \frac{R_{de} - R_{de}^c - (1 - f_l/f_g)R_{dark}}{R_{de}^c}, \quad (3)$$

where R_{de} is the total count rate per one laser pulse period.

As we can see, all of these models describe the afterpulsing to varying degrees of accuracy. The afterpulsing is an internal SPD parameter, and it should not depend on external factors, like laser pulse repetition rate or average energy per laser pulse. Nevertheless, the afterpulsing is a non-markovian process [17], and its probability, obtained with standard methods, will strongly depend on the count rate (see figure 1 d). It means that each of described methods does not allow us to obtain actual internal afterpulse probability.

So these afterpulse models, despite being widely used for QKD systems, have considered disadvantages. However, our priority task is to determine the valid internal afterpulsing parameter, which response to a single triggering. We present the measurement technique and a probabilistic model for estimating the afterpulse based on the recursive nature of this effect. It will allow us to obtain valid internal afterpulsing parameters. We can model our device at any external parameters if we know valid internal parameters, like laser pulse frequency or average laser pulse energy. In the next section, we introduce our model.

III. CUSTOM AFTERPULSE MODELS

Afterpulse is a detection event, that follows a previous detection event, is correlated to a previous detection event, and is not due to photon incident at detectors input [9]. Afterpulse is one of the SPD noise components, like dark counts. Dark counts don't correlate with triggering history and have several causes in the internal SPAD structure: charge band-to-band tunneling, trap-assisted tunneling, thermal generation and other less significant mechanisms [34]. For dark count rate we will use acronym *DCR*.

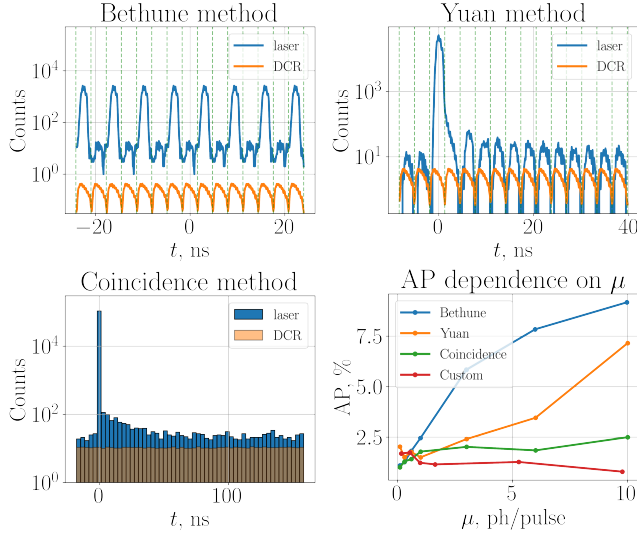


Fig. 1. Afterpulse histogram for different methods: a) the Bethune method ($f_l = 156.25$ MHz); b) the Yuan method ($f_l = 6.25$ MHz); c) the coincidence method ($f_l = 6.25$ MHz); d) the comparison of the afterpulse probability for different methods to laser pulse energy. The green dashed line denotes the gate boundaries. Measurements were performed on custom SPD with the intensity of laser pulses $\mu = 0.1$ ph/pulse.

Afterpulse has the following mechanism: after a detection event, the avalanche quickly quenches, and electrical current through device structure lowers too. After total avalanche quenching, there are a lot of trapped charges in the device structure, that relax with a time. If SPAD bias recovers, than there is high probability to trigger the avalanche due to a detrapped charge. If we forcibly hold the SPAD at off state (with low bias), than after some time, all charges will be detrapped, and new trigger event will not correlate with previous. However, usage of such regime for InGaAs/InP SPAD is impractical, due to high relaxation time. In this case, we have a compromise: if we want low afterpulse, we need to increase hold-off time, but our limiting count rate will lower.

The afterpulse click can trigger the next afterpulse click (second-order afterpulses). This effect is negligible for low afterpulse probabilities ($p_{ap} < 5\%$) but should be carefully accounted for high. In this section, we present two different models – "Simple" and "Complex". The advantage of the simple model is its simplicity and possibility of easy p_{ap} calculation from the statistics. The advantage of the complex model is that it is an accurate statistical description of afterpulse processes in the diode.

Here we assume, that probability of the afterpulse caused an earlier afterpulse is the same as the probability of the afterpulse caused by a laser pulse. We made this assumption in accordance with physical nature of afterpulsing effect. We can't separate clicks, caused by afterpulse, or by laser pulse, because both avalanche processes start with one hole (in InGaAs/InP SPAD) in multiplication region. And there is no additional trapped charge in the heterostructure after the avalanche process, in one of the cases, because both avalanches are on average the same. But if our laser pulses consist of hundreds of photons, most likely we will be able to separate these avalanches. In our model we consider only low-energy

laser pulses ($\approx 0.1 - 10$ photons per pulse), and with high-energy pulses our model is untenable.

The simple model's main idea is the afterpulse click probability P_{ap}^s can be derived from photon-, thermal-, tunneling-induced click probabilities P_0 by the parameter p_{ap}^s . It means, that P_0 consists of light-induced clicks and dark count clicks.

$$P_{ap}^s = P_0 p_{ap}^s. \quad (4)$$

In this view, the P_{ap}^s included the second, third, etc. order afterpulses, and its assessment is included in the parameter p_{ap}^s . This approach is right for the low afterpulse probabilities because the high-order afterpulses are unlikely. The main drawback is that with varying the P_0 by, for example, an increase in the number of photons per pulse, the p_{ap}^s assessment will differ too [15]. We can find the total probability of click P from the schematic diagram 2 a).

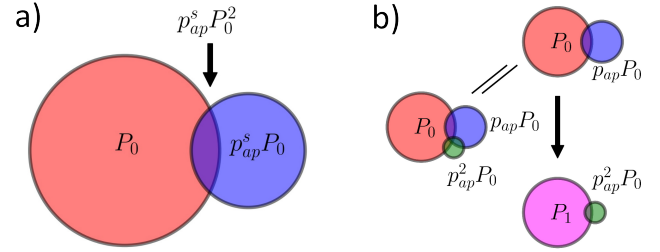


Fig. 2. Schematic diagram of afterpulse probability models: a) simple model; b) complex model. P_0 is a probability of clicking in a system without afterpulse, p_{ap} – is the afterpulse probability.

The total click probability P can be derived as:

$$\text{Simple: } P = P_0 + P_{ap}^s - P_0 P_{ap}^s = P_0(1 + p_{ap}^s - P_0 p_{ap}^s) \quad (5)$$

In the complex model, we take into account the recursive behavior of the afterpulse. In this case, we can show the next schematic diagram, presented in figure 2 b).

The probability that the clicks P_0 will generate an afterpulse is equal to $P_0 p_{ap}$. The probability that afterpulses $P_0 p_{ap}$ generate new afterpulses is $P_0 p_{ap}^2$, and so on. The calculation of the overall afterpulse influence on the total probability of click can be performed by a series of consecutive convolutions of probabilities (P_1, P_2 , etc.). We can write the next equations:

$$\begin{aligned} P_1 &= P_0 + P_0 p_{ap} - P_0 P_0 p_{ap} = P_0(1 - P_0 p_{ap}) + P_0 p_{ap}, \\ P_2 &= P_1 + P_0 p_{ap}^2 - P_1 P_0 p_{ap}^2 = P_1(1 - P_0 p_{ap}^2) + P_0 p_{ap}^2, \\ &\vdots \\ P_{i+1} &= \dots = P_i(1 - P_0 p_{ap}^{i+1}) + P_0 p_{ap}^{i+1}. \end{aligned} \quad (6)$$

This recurrent equation can be rewritten as the decomposition relate parameter P_0 . To do this, we consider the probabilities of afterpulse events as γ_i , where $P(\gamma_i) = P_0 p_{ap}^i$, and these events are joint and independent, which means that $P(\gamma_i \cap \gamma_j) = P(\gamma_i)P(\gamma_j) = P_0^2 p_{ap}^{i+j}$.

$$\begin{aligned}
P_1 &= P(\gamma_0 \cup \gamma_1) = P(\gamma_0) + P(\gamma_1) - P(\gamma_0 \cap \gamma_1) = \\
&= P_0(1 + p_{ap}) - P_0^2 p_{ap}, \\
P_2 &= P(\gamma_0 \cup \gamma_1 \cup \gamma_2) = P(\gamma_0) + P(\gamma_1) + P(\gamma_2) - \\
&- P(\gamma_0 \cap \gamma_1) - P(\gamma_0 \cap \gamma_2) - P(\gamma_1 \cap \gamma_2) + \\
&+ P(\gamma_0 \cap \gamma_1 \cap \gamma_2) = P_0(1 + p_{ap} + p_{ap}^2) - \\
&- P_0^2(p_{ap} + p_{ap}^2 + p_{ap}^3) + P_0^3 p_{ap}^3, \\
&\vdots
\end{aligned} \tag{7}$$

$$\begin{aligned}
P_n &= P(\gamma_0 \cup \gamma_1 \cup \gamma_2 \cup \dots) = P_0 \sum_{i=0}^n p_{ap}^i - \\
&- P_0^2 \sum_{i,j=0;i>j}^n p_{ap}^{i+j} + P_0^3 \sum_{i,j,k=0;k>j>i}^n p_{ap}^{i+j+k} + \dots
\end{aligned}$$

In this recursive equation, P_∞ is the actual probability of the click, which includes all orders of afterpulses. For ease of use in analytical models, we can take the first and second terms in the appropriate order of P_0 . After that, we will analyze the bounds of applicability of these two decomposition models.

We can calculate the sum of the series of first and second order P_0 as follows:

$$\begin{aligned}
\lim_{n \rightarrow \infty} \sum_{i=0}^n p_{ap}^i &= \frac{1}{1 - p_{ap}}, \\
\lim_{n \rightarrow \infty} \sum_{i,j=0;i>j}^n p_{ap}^{i+j} &= \frac{p_{ap}}{(1 - p_{ap})^2(1 + p_{ap})}.
\end{aligned} \tag{8}$$

So, we can derive the first and second-order afterpulse accounting models as:

$$\begin{aligned}
\text{1st order : } P &= P_0 \frac{1}{1 - p_{ap}}, \\
\text{2nd order : } P &= P_0 \frac{1}{1 - p_{ap}} - P_0^2 \frac{p_{ap}}{(1 - p_{ap})^2(1 + p_{ap})}.
\end{aligned} \tag{9}$$

In figure 3, we compare the detection probability P , calculating according to simple, first, second, and high order models. We assume that high-order model (the decomposition of P with 20th order of P_0) is the benchmark, and we should compare the other models to it. We can see that for low afterpulse probability $p_{ap} = 0.1$ all models give good convergence with the high order model, and the low deviations begin with increasing the P_0 . The first model gives the largest error. However, for the higher values of p_{ap} , we can see that simple and first-order have large deviations. Only a second-order model should be used for accurate estimation of total click probability P .

IV. INFLUENCE OF THE ACTIVE RESET ON THE COUNTING STATISTICS

The principal SPD scheme is presented in figure 4. Here, bias generator applies a DC bias, and sine generator applies the sinusoidal bias to SPAD. The sinus frequency is 312.5 MHz. Such frequency used due to SPD was developed to

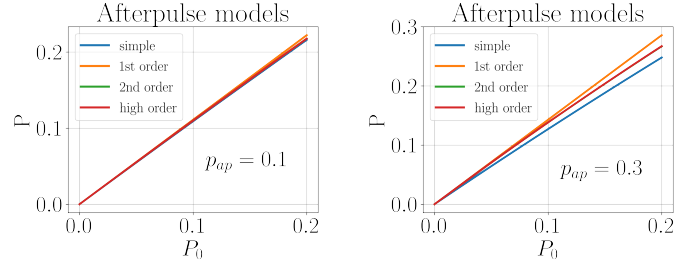


Fig. 3. Comparison of the simple, 1st, 2nd and high order models for determining the click probability P , assuming that a) $p_{ap} = 0.1$, b) $p_{ap} = 0.3$.

use in our QKD device, that works with same laser pulses repetition rate. Arriving photon can trigger the self-sustaining avalanche process, that leads to high current through SPAD and consequent voltage drop can be registered by comparator and classified as click. The quenching process is multistage. The first quenching realized by gated signal – when bias drops below breakdown voltage. After that resistor R_q ($\approx 50 \Omega$) passively quenches the avalanche, that for some time is still growing in the SPAD linear regime. This resistor takes up part of the voltage across the diode, due to sufficiently increased current.

But if we use only the passive quenching, after about hundreds of nanoseconds, the new avalanche processes can occur. It's due to relaxation of DC bias voltage, determined by resistor $R_l \approx 47 k\Omega$, and circuitry and design features of the implementation, introducing parasitic reactances. Moreover, there are a lot of high amplitude relaxation modes after avalanche signal passes through amplifiers and filters block, that can lead to comparator re-triggering (it continues about 100 ns). To prevent this we add a latching to comparator. During latching time τ_l we can't observe SPD triggers, and we can consider it as dead time (we named it "Latched time" (LT)). In figure 4 this regime corresponds to scheme without reset driver, and therefore it's relatively simple for circuit realisation. The main disadvantage is that new avalanches can grow and passively quench during latching time, that sufficiently increases trapped charges, and therefore the afterpulse probability.

To avoid problems with many avalanche triggers during the dead time, after the registration event, we need to use active hold-off time – this is the additional stage in quenching process. We need to note, that this scheme will still be the passive quenching, because first quenching is due to passive elements. Active hold-off enabling delay is about 10 ns after comparator triggering. In figure 4 quenching driver applies the electrical pulse with width τ_c (schematic dead time), that significantly drops the voltage on the SPAD. When SPAD is biased under breakdown, it can't be triggered by single photons, and therefore charge traps continue to relax. The reset to the normal operating regime of the SPAD is due to change of the applying voltage and can be seen as active reset. This dead time realization we named "Latched time + active reset" (LT + AR) [35], [36].

Also, we can define statistical dead time τ_s as the time range

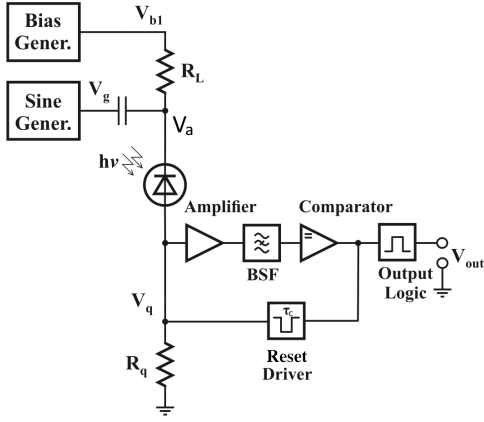


Fig. 4. Functional circuit of SPD. In the circuit: Bias Gener. – DC bias generator; Sine Gener. – AC sinusoidal bias voltage (gate) generator with a frequency of 312.5 MHz; BSF – the filters to eliminate the influence of gates on the processing of avalanche signals.

between some trigger and the next first possible trigger. This time interval depends on τ_l , τ_c , and active reset pulse form. This pulse should be square in the ideal case, but the leading and trailing edges are distorted due to electronics influence.

Trail edge causes high amplitude oscillations, which are difficult to learn due to their high-frequency components, making detector performance difficult to predict. To exclude possible counting of these triggers, we need to make latched time τ_l more than schematic dead time τ_c on the value, approximately equal to the time of these transients τ_{er} . This recovery time can be in the range $200 < \tau_{er} < 3 \mu s$, which depends on the circuit realization, but low values are preferable.

There are different configurations that depend on these time intervals:

- $\tau_l > \tau_c + \tau_{er}$: we present this case in figure 5 a). This figure presents the active reset time and counting statistics for LT and LT + AR schemes (as for the b). Here, latched time fully determines statistical dead time τ_s : $\tau_s = \tau_l$. Here, $\tau_c \approx 3.65 \mu s$ and $\tau_{er} \approx 0.8 \mu s$. The difference $\tau_l - \tau_c - \tau_{er} \approx 0.9 \mu s$. It means that approximately $0.9 \mu s$ in the DT + AR scheme did not detect triggers can occur.
- $\tau_l < \tau_c + \tau_{er}$: we present this case in figure 5 b). Here, $\tau_c \approx 7.5 \mu s$, $\tau_{er} \approx 2.5 \mu s$, $\tau_l \approx 7.8 \mu s$. We can see that the first triggers in the LT + AR scheme occur at $9 \mu s$, which is lower than $\tau_c + \tau_{er} = 10 \mu s$. The statistics are due to the SPD's low detection probability when active reset pulse applied to SPAD and its value < 0 because it lowers the bias voltage. The deviation of the initial section of statistics from the mentioned afterpulse laws is determined by the photon detection efficiency (PDE) dependence on the SPAD bias voltage.

The case, in which using the LT + AR scheme and satisfied $\tau_l \approx \tau_c + \tau_{er}$, where $\tau_{er} \approx 400$ ns is preferable. There are no triggers before the latched time to increase the trap's charge and, consequently, the afterpulse probability. However, setting such a value is a rather non-trivial schematic and technical task.

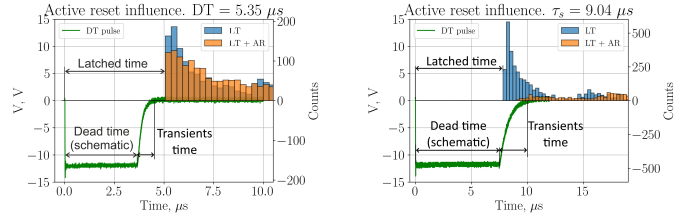


Fig. 5. Active reset influence on the counting statistics: a) $\tau_s = 5.35 \mu s$; b) $\tau_s = 9.04 \mu s$. Two statistics were normalized by zero bin click count $C_0 - C_{dcr}$.

V. AFTERPULSE MEASUREMENT APPROACH

For our measurements we use experimental stand, which principal scheme is presented at figure 6. Black arrows denote electrical connection, yellow denote optical connection. Experimental stand consists of synchronization system, that outputs synchronization signals to high frequency (HF) laser driver, single photon detector and oscilloscope. Due to SPD is gated, we need to synchronize it with laser pulses. HF laser driver controls temperature-stabilized laser, and its output optical laser signal with wavelength $\lambda \approx 1550$ nm, width about 100 ps and FWHM about 40 ps, presented at figure 8 a). In our measurements we used laser pulse repetition rate 10 kHz.

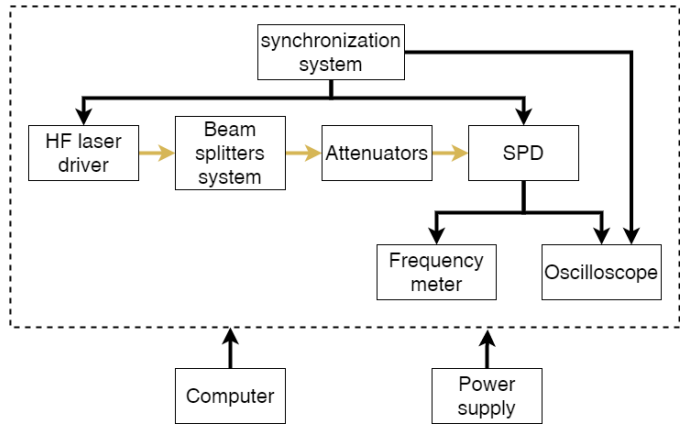


Fig. 6. Functional scheme of SPD's measurement setup: frequency meter – Keysight 53230A, oscilloscope – Lecroy WaveMaster 830Zi-B-R.

Laser pulses arrive to beam splitters system, and one of its outputs connected to attenuators. Other outputs are used to control laser pulse waveform. Attenuators block consists of two devices: first one has output power control, and maintains output power by changing it's attenuation; and the second holds a stable attenuation.

After the attenuators, each laser pulse has mean power about 1 photon. Such signal arrives to SPD, and causes it to be triggered. SPD triggers output electrical signal to frequency meter and oscilloscope. With frequency meter we can evaluate the DCR and PDE parameters, and on oscilloscope time resolution and afterpulse histograms.

By the computer we can control each block of this scheme, instead of beam splitters system, that is passive. Power supply powers each active element.

In our experimental approach, afterpulse measurements can be done by processing the triggers histogram, presented in

figure 7. In the experimental setup, We set the oscilloscope sweep at $25 \mu s$. The detector is most likely to be triggered by laser pulses, and on this detection event oscilloscope will trigger. It's due to the fact that laser pulses period is lower then oscilloscope sweep. But, SPD can be triggered by internal noise, like *DCR* or afterpulsing, and we need to take this into account.

After the trigger click bin, we have empty bins during the dead time. In the detector with LT + AR scheme with well-established latched time of the comparator, new clicks can occur when DC bias voltage fully recovered. With our setup parameters, these clicks most likely are the afterpulses or dark counts, and not the light-induced. In real case, adjustment of latching time is quite complicated, and clicks can occur at growing edge of DC bias. Probability of such clicks is lower, than for fully recovered bias, and we observe this effect on the oscilloscope histograms like reduced some first bins. This effect is not due to poor-quality processing of the histogram. We collect statistics with 10 ns oscilloscope bin with, and after that perform it merging to obtain suitable data representations.

The afterpulse histogram slope could be described by one of the well-researched laws: exponential [37], [38], power-law [39], or hyperbolic sinc model [40], [41]. In these works dead time was established to a fixed value, and afterpulse properties were obtained from histogram analysis. Nevertheless, in practice, this is a non-trivial task to eliminate effect of DC bias recovering influence on click probability, and the first bin after dead time presents this effect. In the third and other dead time windows, previous afterpulse clicks' influence distorts the representation of afterpulse law.

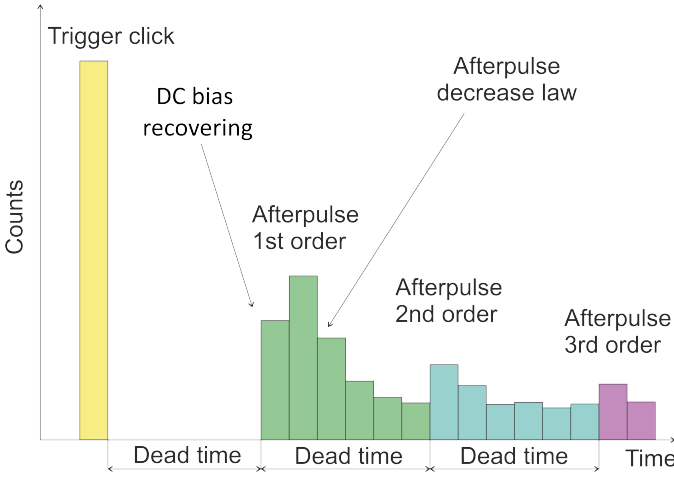


Fig. 7. Schematic collected histogram.

At the figure 8 b) we present the experimental histogram without trigger click bin, that suitable for afterpulse model fitting. First dead time is $\tau = 0.21 \mu s$, and the second $\tau = 7.3 \mu s$. The measurement time for these two histograms is equal, and we can see that for time $t > 8 \mu s$, the bins high slope are roughly the same, which speaks in favor of the exponential afterpulsing law.

At the end of the oscilloscope sweep (the range $t_{dcr} \approx [20, 25] \mu s$), the count of afterpulse clicks will be negligible, and we can consider that it is mainly due to the dark counts.

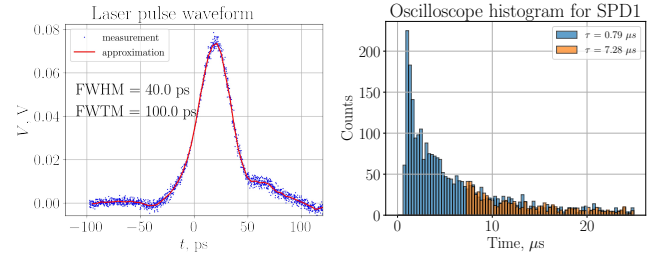


Fig. 8. a) experimental laser pulse waveform; b) experimental histogram of the triggers for SPD1, measured for two different dead times: $\tau = 0.21 \mu s$ and $\tau = 7.3 \mu s$.

There is low probability that photon clicks in this time window because of the last's low repetition rate. We will argue that all counts that differ from the dark counts have afterpulse nature for the rough evaluation. Furthermore, the total afterpulse counts can be found as:

$$C_{dcr} = \frac{1}{N_{dcr}} \sum_{i \in t_{dcr}} C_i, \quad (10)$$

$$C_{ap} = \sum_{i \in [\tau, 25] \mu s} (C_i - C_{dcr}),$$

where C_{dcr} – is the average dark counts accumulated per bin, N_{dcr} – is the bins count in time interval t_{dcr} , C_i – is the count in i -th histogram bin, C_{ap} – is the total counts, that we consider as afterpulse counts (include 1st, 2nd etc. orders).

The C_{ap} counts include different orders of afterpulses. We estimate the afterpulse probability as:

$$p_{ap}^{exp} = \frac{C_{ap}}{C_0}, \quad (11)$$

where the C_0 – is the counts in trigger zero bin of histogram.

The sense of the estimated value can be described by figure 2 a): $p_{ap}^{exp} P_0 \approx P_{ap} - P_{ap} P_0$. Moreover, we can derive the P_{ap} value that should be universal for all models $P_{ap}^{exp} = p_{ap}^{exp} P_0 = P_{ap}$ as:

$$P_{ap} \approx \frac{p_{ap}^{exp} P_0}{1 - P_0} \quad (12)$$

We can easily calculate the p_{ap} for simple, single, and second-order afterpulse models with this assumption. We can relate the p_{ap}^{exp} and p_{ap}^s and p_{ap} parameters:

$$P_{ap} = \frac{P_n - P_0}{1 - P_0},$$

$$p_{ap}^{exp} P_0 = P_n - P_0, \quad (13)$$

$$P_n = P_0(1 + p_{ap}^{exp}),$$

where we obtained the right-hand side for the first equation from the simple equation for P_n (P notation for simple model) probability: $P_n = P_0 + P_{ap} - P_0 P_{ap}$. The P and P_n can be derived from equations 5 and 9 for simple, first and second-order models.

For the simple and first order models, we can get the simple relation for p_{ap}^s and $p_{ap}^{(1)}$:

$$p_{ap}^s = \frac{p_{ap}^{exp}}{1 - P_0}, \quad (14)$$

$$p_{ap}^{(1)} = 1 - \frac{1}{1 + p_{ap}^{exp}}.$$

Similarly, we can find the $p_{ap}^{(2)}$ for the second-order model, but this is a non-trivial task to do it analytically. For this reason, $p_{ap}^{(2)}$ can be found only numerically.

We can find the $p_{ap}^{(1)}$ value from experimental p_{ap}^{exp} , but to calculate the p_{ap}^s and $p_{ap}^{(2)}$, we need to find the P_0 probability previously. To do this, we need to know the overall probability of click P_n (or P for simple model), which we can find from count rate R and dead time (statistical) τ : $P_n = R\tau$ [42]. After that, we need to paste it into equation 5 or 9 (depends on the observed model) and calculate the P_0 . For the simple model, we can derive the p_{ap}^s value from R analytically:

$$p_{ap}^s = \frac{p_{ap}^{exp}(1 + p_{ap}^{exp})}{1 + p_{ap}^{exp} - R\tau}. \quad (15)$$

It is evident that with low $R\tau$ the equation 15 takes the following form: $p_{ap}^s = p_{ap}^{exp}$.

For accurate SPD models, one should use the second-order model because $p_{ap}^{(2)}$ does not depend on the P_0 , and one value of $p_{ap}^{(2)}$ can be used for a wide range of optical power per pulse μ (ph/pulse). The simple model is suitable only for low values of p_{ap}^s , and when SPD operation is proposed only with fixed μ . First-order model suits in the case of low $p_{ap}^{(1)}$ because, like for the 2nd order model, it can be used for wide (but lower than for 2nd model) range μ , and simple form of equations allows you to use it in analytical models of SPD.

VI. RESULTS

We tested three custom sinusoidal gated SPDs based on InGaAs/InP SPADs named SPD1, SPD2, and SPD3. These SPADs (with gated frequency $\nu = 312.5$ MHz) were manufactured by Wooriro company and were taken from different batches. The SPAD №2 and №3 have butterfly housing and a built-in enclosure cooling system. We have shown its main parameters in table I.

TABLE I
PARAMETERS OF USED SPADS.

SPD №	SPAD	T , K	DCR, Hz ($\tau \approx 20 \mu s$)	
			$PDE = 10 \%$	$PDE = 20 \%$
1	PA19H262-0004	223	≈ 250	≈ 450
2	MF20C300-0001	233	≈ 50	≈ 100
3	MF20D300-0001	233	≈ 150	≈ 300

We added the possibility of enabling or disabling reset driver (passive-active quenching and reset) to the circuit realization of SPD. Also, we added the manual setting of the circuit dead time τ_c and latching time τ_l . In all presented below figures, it was $\tau_l > \tau_c$. However, due to transients at the trailing edge during the τ_{er} , we cannot accurately set the parameters to achieve the preferable condition: $\tau_l > \tau_c + \tau_{er}$. For this reason,

some data was obtained for the first case and another for the second case of time interval configurations, presented above. It means that statistical dead time τ_s for LT and LT + AR schemes can differ for the similar setting of latched time.

In our experiments, laser pulses with FWHM ≈ 50 ps and repetition rate 10 kHz were attenuated to the average power per pulse $\mu \approx 1$ ph/pulse. We established two PDE in our experiments: 10 % and 20 %. The setting of the PDE value was performed by changing the SPD's bias voltage with unchanged gate amplitude. The statistics was collected on an oscilloscope and processed to obtain p_{ap}^{exp} value. After that, we found p_{ap}^s , $p_{ap}^{(1)}$ and $p_{ap}^{(2)}$, which correspond to simple, first, and second-order models.

In figure 9 a), we present the p_{ap} value for LT and LT + AR schemes obtained for simple and second-order models (diamond and point markers correspondingly). We approximated data for SPD1 and SPD2 curves defined by the power-law equation. Data for SPD3 was approximated with an exponential equation:

$$\begin{aligned} \text{power law: } p_{ap}^{pl}(\tau) &= A\tau^B + C, \\ \text{exponential: } p_{ap}^e(\tau) &= Ae^{-B\tau} + C, \end{aligned} \quad (16)$$

where the A , B and C parameters have been fitted.

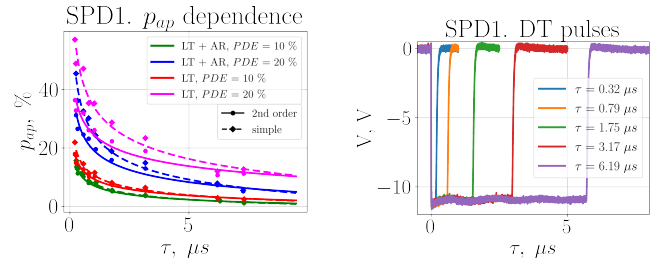


Fig. 9. SPD1 data: a) Comparing p_{ap} for LT and LT + AR schemes, obtained in according to simple and second-order models (diamonds and points correspondingly). Dashed lines represent the fitted curves for simple model, solid lines – for the second-order model; b) Active reset pulse, applied to SPAD after the trigger.

The common used law for approximate the p_{ap} dependence on the dead time for fixed PDE is the exponential, as shown in works [34], [35], [43]–[47]. But in our work we fixed the total counts R , that can be considered as fixed PDE only for low p_{ap} (the SPD3 has low p_{ap} and data had been approximated with exponential law quite well). We didn't fix the PDE value instead because there is not consensus for it's definition equation. On contrary, experimentally obtained counting rates can be defined only one way.

In this figure, we can see that afterpulse probability estimation p_{ap} at the high values and low τ values sufficiently differs for simple and second-order models – solid and dashed curves. However, for low p_{ap} and high τ they almost coincide. We can see that using active reset has significant effects on the p_{ap} , which is especially noticeable for $PDE = 20 \%$. We can also see that with higher bias voltage on SPAD, which is directly related to R , the afterpulse probability is high.

Figure 9 b) presents the active reset pulses. The leading edge is sharp in order to remove possible triggers that may

occur quickly. In this case, high-amplitude transient processes occur, but they do not influence triggers. The trailing edge is smoother to reduce the internal transients' time interval and make its amplitude lower.

Figure 10 is similar to figure 9 but performed for SPD2. We can see that for $PDE = 20\%$, p_{ap} is sufficiently higher than p_{ap} for SPD1, and vice versa for $PDE = 10\%$. This feature is not due to the control circuit but due to differences in the SPAD's characteristics. In figure b), we can see that the trailing edge is sufficiently smoother. For SPD1, that can cause intense manifestation of lowering the detector click probability due to DC bias recovering and therefore reduce SPAD efficiency for high-frequency laser pulse repetition rates.

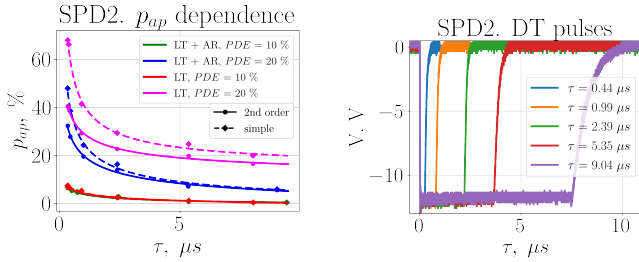


Fig. 10. SPD2 data: a) Comparing p_{ap} for LT and LT + AR schemes, obtained in according to simple and second-order models (diamonds and points correspondingly). Dashed lines represent the fitted curves for simple model, solid lines – for the second-order model; b) Active reset pulse, applied to SPAD after the trigger.

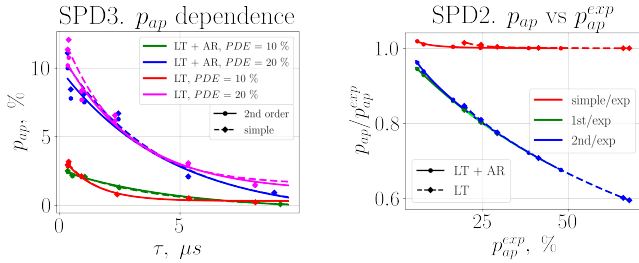


Fig. 11. a) SPD3 data: comparing of p_{ap} for LT and LT + AR schemes, obtained in according to simple and second-order models (diamonds and points correspondingly). Dashed lines represent the fitted curves for simple model, solid lines – for the second-order model; b) SPD2 data: comparing of p_{ap}^s , $p_{ap}^{(1)}$ and $p_{ap}^{(2)}$ with p_{ap}^{exp} for the SPD2 data and $PDE = 20\%$.

Figure 11 a) presents the same, as in figures 9 and 10, but for SPD3 data. The afterpulse probability for this detector is small enough even for low dead time and disabled active reset. For the $PDE = 10\%$ data, the LT red curve lies lower than LT + AR green curve. Here it is already a matter of measurement errors and the features of the approximation of experimental data.

Figure 11 b) compares the p_{ap}^s , $p_{ap}^{(1)}$ and $p_{ap}^{(2)}$ with p_{ap}^{exp} for the SPD2 data and $PDE = 20\%$. We can see that the first and second-order models have a satisfactory agreement for high afterpulse probabilities and sufficiently differ from experimentally obtained p_{ap}^{exp} . These models differ for the afterpulse probability $p_{ap}^{exp} < 15\%$. The simple model for a high $p_{ap}^{exp} > 15\%$ tends to this p_{ap}^{exp} value. However, for a lower p_{ap}^{exp} , it has even more value. There is no sufficient

difference between the LT or LT + AR schemes – they converge quite well on these graphs.

We can make the main conclusions of this schedule:

- There is no difference in p_{ap} for the LT and LT + AR schemes for high τ values and low R (related with PDE) rates. If SPD is not designed with strict requirements for limiting count rates and quantum efficiency, then it is permissible not to use a circuit with active reset pulses.
- Choosing a model for calculating the p_{ap} is essential for high afterpulse probabilities ($p_{ap}^{exp} > 5\%$) – first, or second-order models are preferable. For low values p_{ap}^{exp} , we can use a simple model too. According to the simple model, we get a strongly overestimated value of the afterpulse, which coincides with the experimentally found one.

VII. CONCLUSION

The main result of the work is that we compare schemes with latching time (LT) and with latching time and active reset (LT + AR) and its influence on the afterpulse probability. As a result of the experiments, we have shown that an active reset module could significantly reduce afterpulse probability. However, with extensive dead time ($\tau > 10 \mu s$) and generally low afterpulse probabilities ($p_{ap}^{exp} < 5\%$), the differences between the two schemes are relatively insignificant. With low requirements for the detector ($\tau > 5 \mu s$ and $PDE = 10\%$), the possibility of abandoning the active reset module will significantly simplify the detector's circuit design. At the same time, it slightly increases the afterpulse probability. We must mention that we performed our measurements on the 10 kHz laser pulses repetition rate. In the LT scheme, afterpulse probability will sufficiently increase for high laser pulse repetition rates (> 1 MHz) due to generating additional avalanche processes during the latching time. Also, we give recommendations for setting the values of the circuit dead time and latching time from the conditions of the internal transient time.

The second result is the developed approach to determining the probability of afterpulses of detectors, following three models. We have described the procedure for processing statistics from the oscilloscope histograms to obtain the experimental afterpulse probability. We introduce three models: simple, 1-st, and 2-nd order. A simple model is not appropriate for describing the afterpulsing counting statistics due to rough underlying physical processes. As a result of the experiments, we have shown that using the simple model gives rough results, which at high afterpulse probabilities simplify experimentally obtained values. We have shown that it is best to use the second-order model, which should give correct results for both small and large afterpulse probabilities. If the use of the analytical applications model is required, then the first-order model should be used because of its simple algebraic form. We have obtained that results have minor deviations from the second-order model with the afterpulse probability $p_{ap}^{exp} < 15\%$, but for large values, they coincide well. We have compared our afterpulsing measurement approach with other commonly used models like Bethune method [19], Yuan

method [20], and coincidence method [23]. We have shown that the afterpulse probability obtained with our method is less sensitive to the laser pulses power changes.

REFERENCES

- [1] L. You, "Superconducting nanowire single-photon detectors for quantum information," *Nanophotonics*, vol. 9, no. 9, pp. 2673–2692, 2020.
- [2] C. Bruschini, H. Homulle, and E. Charbon, "Ten years of biophotonics single-photon SPAD imager applications: retrospective and outlook," in *Multiphoton Microscopy in the Biomedical Sciences XVII*, vol. 10069. International Society for Optics and Photonics, 2017, p. 100691S.
- [3] J. Chang, J. Los, J. Tenorio-Pearl, N. Noordzij, R. Gourgues, A. Guardiani, J. Zichi, S. Pereira, H. Urbach, V. Zwiller, S. Dorenbos, and E. Zadeh, "Detecting telecom single photons with 99.5- 2.07+ 0.5% system detection efficiency and high time resolution," *APL Photonics*, vol. 6, no. 3, p. 036114, 2021.
- [4] C. Agnesi, M. Avesani, L. Calderaro, A. Stanco, G. Foletto, M. Zahidy, A. Scriminich, F. Vedovato, G. Vallone, and P. Villoresi, "Simple quantum key distribution with qubit-based synchronization and a self-compensating polarization encoder," *Optica*, vol. 7, no. 4, pp. 284–290, 2020.
- [5] Z. Zhang, C. Chen, Q. Zhuang, F. N. Wong, and J. H. Shapiro, "Experimental quantum key distribution at 1.3 gigabit-per-second secret-key rate over a 10 dB loss channel," *Quantum Science and Technology*, vol. 3, no. 2, p. 025007, 2018.
- [6] J.-P. Chen, C. Zhang, Y. Liu, C. Jiang, W. Zhang, X.-L. Hu, J.-Y. Guan, Z.-W. Yu, H. Xu, J. Lin, M.-J. Li, H. Chen, H. Li, L. You, Z. Wang, X.-B. Wang, Q. Zhang, and J.-W. Pan, "Sending-or-not-sending with independent lasers: Secure twin-field quantum key distribution over 509 km," *Physical review letters*, vol. 124, no. 7, p. 070501, 2020.
- [7] E. O. Kiktenko, N. O. Pozhar, A. V. Duplinskiy, A. A. Kanapin, A. S. Sokolov, S. S. Vorobey, A. V. Miller, V. E. Ustimchik, M. N. Anufriev, A. Trushechkin, R. Yunusov, V. Kurochkin, Y. Kurochkin, and A. Fedorov, "Demonstration of a quantum key distribution network in urban fibre-optic communication lines," *Quantum Electronics*, vol. 47, no. 9, p. 798, 2017.
- [8] L.-Y. Zhao, Q.-J. Wu, H.-K. Qiu, J.-L. Qian, and Z.-F. Han, "Practical security of wavelength-multiplexed decoy-state quantum key distribution," *Physical Review A*, vol. 103, no. 2, p. 022429, 2021.
- [9] C. Wang, J. Wang, Z. Xu, J. Li, R. Wang, J. Zhao, and Y. Wei, "Afterpulsing effects in SPAD-based photon-counting communication system," *Optics Communications*, vol. 443, pp. 202–210, 2019.
- [10] H. Wang, H. Li, L. You, Y. Wang, L. Zhang, X. Yang, W. Zhang, Z. Wang, and X. Xie, "Fast and high efficiency superconducting nanowire single-photon detector at 630 nm wavelength," *Applied optics*, vol. 58, no. 8, pp. 1868–1872, 2019.
- [11] S. C. Wein, J.-W. Ji, Y.-F. Wu, F. K. Asadi, R. Ghobadi, and C. Simon, "Analyzing photon-count heralded entanglement generation between solid-state spin qubits by decomposing the master-equation dynamics," *Physical Review A*, vol. 102, no. 3, p. 033701, 2020.
- [12] E. Sarbazi, M. Safari, and H. Haas, "The impact of long dead time on the photocount distribution of SPAD receivers," in *2018 IEEE Global Communications Conference (GLOBECOM)*. IEEE, 2018, pp. 1–6.
- [13] M. A. Smirnov, N. S. Perminov, R. R. Nigmatullin, A. A. Talipov, and S. A. Moiseev, "Sequences of the ranged amplitudes as a universal method for fast noninvasive characterization of SPAD dark counts," *Applied optics*, vol. 57, no. 1, pp. 57–61, 2018.
- [14] D. Kramnik and R. J. Ram, "Efficient statistical separation of primary dark counts and afterpulses in free-running SPADs," in *CLEO: Applications and Technology*. Optical Society of America, 2020, pp. JTh2A–29.
- [15] G.-J. Fan-Yuan, J. Teng, S. Wang, Z.-Q. Yin, W. Chen, D.-Y. He, G.-C. Guo, and Z.-F. Han, "Optimizing single-photon avalanche photodiodes for dynamic quantum key distribution networks," *Physical Review Applied*, vol. 13, no. 5, p. 054027, 2020.
- [16] P. Owens, J. Rarity, P. Tapster, D. Knight, and P. Townsend, "Photon counting with passively quenched germanium avalanche," *Applied Optics*, vol. 33, no. 30, pp. 6895–6901, 1994.
- [17] F.-X. Wang, W. Chen, Y.-P. Li, D.-Y. He, C. Wang, Y.-G. Han, S. Wang, Z.-Q. Yin, and Z.-F. Han, "Non-markovian property of afterpulsing effect in single-photon avalanche detector," *Journal of Lightwave Technology*, vol. 34, no. 15, pp. 3610–3615, 2016.
- [18] Y. Kang, D. Bethune, W. Risk, and Y.-H. Lo, "Afterpulsing of single-photon avalanche photodetectors," in *The 16th Annual Meeting of the IEEE Lasers and Electro-Optics Society, 2003. LEOS 2003.*, vol. 2. IEEE, 2003, pp. 775–776.
- [19] D. S. Bethune, W. P. Risk, and G. W. Pabst, "A high-performance integrated single-photon detector for telecom wavelengths," *Journal of modern optics*, vol. 51, no. 9-10, pp. 1359–1368, 2004.
- [20] Z. Yuan, B. Kardynal, A. Sharpe, and A. Shields, "High speed single photon detection in the near infrared," *Applied Physics Letters*, vol. 91, no. 4, p. 041114, 2007.
- [21] N. Namekata, S. Adachi, and S. Inoue, "1.5 GHz single-photon detection at telecommunication wavelengths using sinusoidally gated InGaAs/InP avalanche photodiode," *Optics express*, vol. 17, no. 8, pp. 6275–6282, 2009.
- [22] Y. Nambu, S. Takahashi, K. Yoshino, A. Tanaka, M. Fujiwara, M. Sasaki, A. Tajima, S. Yorozu, and A. Tomita, "Efficient and low-noise single-photon avalanche photodiode for 1.244-GHz clocked quantum key distribution," *Optics express*, vol. 19, no. 21, pp. 20 531–20 541, 2011.
- [23] J. Zhang, R. Thew, C. Barreiro, and H. Zbinden, "Practical fast gate rate InGaAs/InP single-photon avalanche photodiodes," *Applied Physics Letters*, vol. 95, no. 9, p. 091103, 2009.
- [24] J. Zhang, P. Eraerds, N. Walenta, C. Barreiro, R. Thew, and H. Zbinden, "2.23 GHz gating InGaAs/InP single-photon avalanche diode for quantum key distribution," in *Advanced Photon Counting Techniques IV*, vol. 7681. International Society for Optics and Photonics, 2010, p. 76810Z.
- [25] Y. Zhang, X. Zhang, Y. Shi, Z. Ying, and S. Wang, "Electro-optic modulator based gate transient suppression for sine-wave gated InGaAs/InP single photon avalanche photodiode," *Optical Engineering*, vol. 53, no. 6, p. 067102, 2014.
- [26] A. Restelli, J. C. Bienfang, and A. L. Migdall, "Time-domain measurements of afterpulsing in InGaAs/InP SPAD gated with sub-nanosecond pulses," *Journal of Modern Optics*, vol. 59, no. 17, pp. 1465–1471, 2012.
- [27] M. A. Itzler, X. Jiang, M. Entwistle, K. Slomkowski, A. Tosi, F. Acerbi, F. Zappa, and S. Cova, "Advances in InGaAsP-based avalanche diode single photon detectors," *Journal of Modern Optics*, vol. 58, no. 3-4, pp. 174–200, 2011.
- [28] J. Zhang, R. Thew, J.-D. Gautier, N. Gisin, and H. Zbinden, "Comprehensive characterization of InGaAs–InP avalanche photodiodes at 1550 nm with an active quenching ASIC," *IEEE Journal of Quantum Electronics*, vol. 45, no. 7, pp. 792–799, 2009.
- [29] S. Arahira and H. Murai, "Effects of afterpulse events on performance of entanglement-based quantum key distribution system," *Japanese Journal of Applied Physics*, vol. 55, no. 3, p. 032801, 2016.
- [30] D. N. Klyshko, "Use of two-photon light for absolute calibration of photoelectric detectors," *Soviet Journal of Quantum Electronics*, vol. 10, no. 9, pp. 1112–1117, Sep 1980.
- [31] P. G. Kwiat, A. M. Steinberg, R. Y. Chiao, P. H. Eberhard, and M. D. Petroff, "Absolute efficiency and time-response measurement of single-photon detectors," *Applied optics*, vol. 33, no. 10, pp. 1844–1853, 1994.
- [32] G. Brida, S. Castelletto, I. P. Degiovanni, C. Novero, and M. L. Rastello, "Quantum efficiency and dead time of single-photon counting photodiodes: a comparison between two measurement techniques," *Metrologia*, vol. 37, no. 5, p. 625, 2000.
- [33] S. V. Polyakov and A. L. Migdall, "High accuracy verification of a correlated-photon-based method for determining photon-counting detection efficiency," *Optics Express*, vol. 15, no. 4, pp. 1390–1407, 2007.
- [34] A. Tosi, N. Calandri, M. Sanzaro, and F. Acerbi, "Low-noise, low-jitter, high detection efficiency InGaAs/InP single-photon avalanche diode," *IEEE Journal of selected topics in quantum electronics*, vol. 20, no. 6, pp. 192–197, 2014.
- [35] J. Liu, Y. Xu, Y. Li, Y. Gu, Z. Liu, and X. Zhao, "Ultra-low dead time free-running InGaAsP single-photon detector with active quenching," *Journal of Modern Optics*, vol. 67, no. 13, pp. 1184–1189, 2020.
- [36] J. Liu, Y. Xu, Y. Li, Z. Liu, and X. Zhao, "Exploiting the single-photon detection performance of InGaAs negative-feedback avalanche diode with fast active quenching," *Optics Express*, vol. 29, no. 7, pp. 10 150–10 161, 2021.
- [37] B. Korzh, T. Lunghi, K. Kuzmenko, G. Boso, and H. Zbinden, "Afterpulsing studies of low-noise InGaAs/InP single-photon negative-feedback avalanche diodes," *Journal of Modern Optics*, vol. 62, no. 14, pp. 1151–1157, 2015.
- [38] G. Humer, M. Peev, C. Schaeff, S. Ramelow, M. Stipčević, and R. Ursin, "A simple and robust method for estimating afterpulsing in single photon detectors," *Journal of Lightwave Technology*, vol. 33, no. 14, pp. 3098–3107, 2015.
- [39] M. A. Itzler, X. Jiang, and M. Entwistle, "Power law temporal dependence of InGaAs/InP SPAD afterpulsing," *Journal of Modern Optics*, vol. 59, no. 17, pp. 1472–1480, 2012.
- [40] D. Horoshko, V. Chizhevsky, and S. Y. Kilin, "Afterpulsing model based on the quasi-continuous distribution of deep levels in single-photon

- avalanche diodes,” *Journal of Modern Optics*, vol. 64, no. 2, pp. 191–195, 2017.
- [41] A. W. Ziarkash, S. K. Joshi, M. Stipčević, and R. Ursin, “Comparative study of afterpulsing behavior and models in single photon counting avalanche photo diode detectors,” *Scientific reports*, vol. 8, no. 1, pp. 1–8, 2018.
- [42] A. Koziy, A. Tayduganov, A. Losev, V. Zavodilenko, A. Gorbatshevich, and Y. Kurochkin, “Investigating the coherent state detection probability of InGaAs/InP SPAD-based single-photon detectors,” 2021.
- [43] J. C. Campbell, W. Sun, Z. Lu, M. A. Itzler, and X. Jiang, “Common-mode cancellation in sinusoidal gating with balanced InGaAs/InP single photon avalanche diodes,” *IEEE Journal of Quantum Electronics*, vol. 48, no. 12, pp. 1505–1511, 2012.
- [44] J. Liu, Y. Li, L. Ding, Y. Wang, T. Zhang, Q. Wang, and J. Fang, “Fast active-quenching circuit for free-running InGaAs (P)/InP single-photon avalanche diodes,” *IEEE Journal of Quantum Electronics*, vol. 52, no. 10, pp. 1–6, 2016.
- [45] J. Liu, T. Zhang, Y. Li, L. Ding, J. Tao, Y. Wang, Q. Wang, and J. Fang, “Design and characterization of free-running InGaAsP single-photon detector with active-quenching technique,” *Journal of Applied Physics*, vol. 122, no. 1, p. 013104, 2017.
- [46] J. Kirdoda, D. C. Dumas, R. W. Millar, M. M. Mirza, D. J. Paul, K. Kuzmenko, P. Vines, Z. Greener, and G. S. Buller, “Geiger mode Ge-on-Si single-photon avalanche diode detectors,” in *2019 IEEE 2nd British and Irish Conference on Optics and Photonics (BICOP)*. IEEE, 2019, pp. 1–4.
- [47] Y.-Q. Fang, W. Chen, T.-H. Ao, C. Liu, L. Wang, X.-J. Gao, J. Zhang, and J.-W. Pan, “InGaAs/InP single-photon detectors with 60% detection efficiency at 1550 nm,” *Review of Scientific Instruments*, vol. 91, no. 8, p. 083102, 2020.